Computational Materials Science 200 (2021) 110804

Contents lists available at ScienceDirect

Computational Materials Science

journal homepage: www.elsevier.com/locate/commatsci

Thermally-activated dislocation mobility in bcc metals: An accelerated molecular dynamics study

Blazej Grabowski *, Nikolay Zotov

Institute for Materials Science, University of Stuttgart, Pfaffenwaldring 55, 70569 Stuttgart, Germany

ARTICLE INFO

Keywords:
Accelerated molecular dynamics
Screw dislocations
Bcc Nb
Kink-pairs
Activation Gibbs energy

ABSTRACT

Plastic deformation in metals is controlled by dislocation density and mobility. In bcc metals the mobility of screw dislocations, which takes place by temperature- and stress-driven nucleation of critical kink-pairs, is most essential for deformation. However, the critical resolved shear stresses at low temperatures, as determined from molecular dynamics (MD) simulations performed at constant strain rate, are typically 2–3 times larger than the yield stresses measured experimentally. Here, an accelerated MD procedure is developed and employed to investigate the *onset* of dislocation mobility in the prototypical system bcc Nb. The method combines constant strain and temperature MD with hyperdynamics, using a bond-boost potential. We demonstrate, with a careful statistical analysis, that the method enables nucleation of critical kink-pairs and the determination of the Gibbs energy of kink-pair formation from accelerated MD simulations at experimentally-measured shear stresses.

1. Introduction

Dislocations play a critical role in the plastic deformation (yielding) of metals. The yield stress for most metals is much lower than the theoretical 'ultimate' stress [1] due to the presence and movement of dislocations via dislocation slip. Bcc transition metals show, in comparison with fcc metals, a strong temperature- and strain dependence of the yield stress (the critical resolved shear stress τ^*, CRSS) [2,3] at low temperatures, due to the large and anisotropic lattice resistance (Peierls barriers) for the glide of ½ [1 1 1] screw dislocations in these materials. The rate equation for the yield stress τ^*, controlled by thermal fluctuations, can be generally written as:

$$\dot{\gamma} = \dot{\gamma}_0 \exp(-\Delta G(\tau^*)/k_B T), \tag{1a}$$

where $\dot{\gamma}$ is the plastic shear strain rate, $\Delta G(\tau^*)$ the Gibbs energy for dislocation motion at a given CRSS, and k_B the Boltzmann constant. The entropy contribution is generally believed to be a small fraction of the total Gibbs energy and Eq. (1a) is commonly simplified to [3,4]:

$$\dot{\gamma} = \dot{\gamma}_0 \exp(-\Delta H(\tau^*)/k_B T), \tag{1b}$$

where $\Delta H(\tau^*)$ is the activation enthalpy for dislocation motion. The pre-exponential factor $\dot{\gamma}_0$ is usually taken equal to $b\rho_m \nu d$, where b is the length of the Burgers vector, ρ_m is the density of mobile dislocations per unit dislocation length, ν is a characteristic frequency in the order of the Debye frequency and d is the distance between two Peierls valleys. The activation enthalpy $\Delta H(\tau^*)$ can be determined from experiments using the strain-rate dependence of the CRSS [4] and is of the order of $30k_BT$ [4], but generally cannot be identified with a *single* atomistic process.

On the other hand, significant understanding on the *atomistic level* of the structure and the glide mechanisms of ½ [1 1 1] screw dislocations in bcc metals has been obtained using molecular static and dynamic simulations [5]. However, all classical atomistic simulations of bcc metals with dislocations, starting 50 year ago with the study on bcc Na [6], predict Peierls stresses (at $T = 0$ K) and CRSS at higher temperatures by a factor 2 to 3 larger than experimental values [7–12]. Gröger and Vitek [13] proposed an explanation for the discrepancy between the experimentally measured and the simulated Peierls stresses, based on the idea that in macroscopic experiments there are always Frank-Read sources emitting dislocations with non-screw components, so that groups of interacting non-screw and screw dislocations can start moving at lower applied stresses. This model, however, does not take into account that classical MD simulations are performed typically at shear strain rates that are 12 orders of magnitude larger than in experiments. Strain rates in MD simulations have to be in the order of 10^6–10^9 s^{-1} to achieve strains of any physical significance, while typical laboratory deformation experiments are carried out at much lower shear strain rates in the range of 10^{-4}–10^{-1} s^{-1} [3,4,14].

* Corresponding author.
E-mail address: blazej.grabowski@imw.uni-stuttgart.de (B. Grabowski).

https://doi.org/10.1016/j.commatsci.2021.110804
Received 17 May 2021; Received in revised form 21 July 2021; Accepted 13 August 2021
Available online 13 September 2021

Generally, the experimentally-obtained CRSS increases with decreasing temperature and increasing strain rate [3,4]. Phenomenological thermodynamic models, based on Eq. (1b), lead to a logarithmic dependence of the thermally-activated shear stress τ on the strain rate [15,16]:

$$\tau = \tau_0 A(T)[1 + B(T)\ln(\dot{\gamma}/\dot{\gamma}_0)], \quad (2)$$

where A and B are temperature-dependent material (or fit) constants. Considering the many orders of magnitude larger strain rates in MD simulations, Eq. (2) shows clearly that any such brute-force MD simulation will inevitably lead to a much larger CRSS.

In MD simulations performed at a constant strain rate, the CRSS, denoted hereafter τ_c, is determined as the critical stress during shearing at which an isolated screw dislocation starts to move. This event takes place at a given critical MD time t_c. The critical time t_c (and the corresponding computational run time) increases rapidly with decreasing shear strain rate (see Sec. 4.1), which makes impossible the execution of classical MD simulations at experimental shear strain rates in reasonable computational time frames.

Several methods for *accelerated* MD simulations have been proposed in the literature (see e.g. Ref. [17] for an overview), beginning with the seminal work of Voter [18] in 1997 on the hyperdynamics (HD) method. Acceleration methods in general focus on processes where the long-time evolution consists of infrequent transitions from one to another equilibrium state without correlations between successive state-to-state transitions (*random rare events*). The HD method, in particular, is based on a modification of the potential energy surface by addition of a positive boost potential ΔV_b to the equilibrium state basins, which reduces the potential barrier for state-to-state transitions. Unfortunately, it is not possible to devise a general boost potential that captures all types of rare events.

In metals, the HD method has been therefore tested only on rather simple small-size systems with well-defined transitions like adatom diffusion on metal surfaces [19–21], using a bond boost potential [19]. In these studies: (i) the activation volume of the transition state involves only several atoms, (ii) the sequence and the direction of the adatom jumps from one lattice site to another are not correlated (only thermally activated) and (iii) the adatom jumps involve bond-breaking and reconstruction between nearest neighbours, which is the main ingredient of the bond-boost method [19].

The original HD method [18] is applicable only to non-driven processes. However, more complicated deformation processes of interest in material science and physics are not only thermally-activated but strain- or stress-driven as well, and they involve relatively large number of atoms as well as collective, cooperative events like the nucleation of kink pairs [22]. This is the reason why, up to now, only very few studies have applied HD (or modifications of it) to metal systems. Specifically, dislocation nucleation in Cu and Ni has been investigated [23–25]. However, in pure fcc metals the Peierls stress is negligible (<2 MPa) and the dislocation mobility is much faster [3].

In the present work, we develop a method that enables a controlled acceleration of dislocations in MD simulations, and we demonstrate its performance for the prototype case of screw dislocation mobility in bcc metals, specifically Nb, by successfully obtaining critical shear stresses typical for macroscopic deformation experiments. We consider Nb, mainly because Nb has the lowest shear modulus along the [1 1 1] direction [3] and the lowest enthalpy of critical KP formation [22] among all bcc transition metals. Thus, it can be expected that Nb exhibits (relatively) high KP nucleation rates, more easily accessible with MD simulations.

2. Computational details

The simulations were performed on a dipole model, containing 48,000 Nb atoms and initially two straight screw dislocations with opposite Burgers vectors, both at 'easy-core' positions.

The model was generated using the ATOMSK program [26]. The crystallographic directions along the supercell axis were $X \,||\, [01\bar{1}]$, $Y \,||\, [111]$ and $Z \,||\, [2\bar{1}\,\bar{1}]$ (see Fig. 1a), corresponding to the $(2\bar{1}\,\bar{1})$ maximum resolved shear stress (MRSS) plane. The simulation supercell had dimensions of $L_x = 187$Å, $L_y = 10b = 28.6$Å and $L_z = 162$Å, $b = 2.86$ Å for bcc Nb. The dipole model allows periodic boundary conditions to be imposed along all three directions X, Y and Z, with the screw dislocations lying parallel to the Y axis.

The length of the Y axis was selected in such a way that typically nucleation of only one critical KP on the dislocation line was observed. A constant shear along the Y axis was applied to the simulation cell at each time step, thus enabling simulations at a given constant shear strain rate over time, which is commonly used in experiments. In order to determine the rate dependence of the critical waiting time t_c, standard MD simulations were performed at several strain rates from 1×10^6 to 1×10^8 s^{-1} using at least 10 different initial velocity distributions. For the simulations in the strain-reduction setup (described in the following section) the initial strain rate to reach the reduced strain was set to 1×10^8 s^{-1}. It should be noted that, generally, a pure shear strain deformation does not lead to a pure shear stress state and *vice versa* a pure shear stress deformation does not lead to a pure shear strain state, unless the material is isotropic [27]. In our shearing simulations, we observed very weak $(0.002G_{\{111\}})$ stresses $\sigma_{XX} = -\sigma_{ZZ}$, which arise from the non-zero elastic constant c'_{14} in the coordinate system defined by the vectors of the simulation supercell, where $G_{\{111\}} = \frac{1}{3}(c_{11} - c_{12} + c_{44})$ is the shear modulus along the [1 1 1] direction [2]. c'_{14} can be expressed in terms of c_{44} and the anisotropy (Zener) ratio $A = \frac{2c_{44}}{c_{11}-c_{12}}$ as $c'_{14} = c_{44}(1 - A)/2A$. This expression shows that shearing of elastically-anisotropic metals ($A \neq 1$), like Nb, inevitably leads to such an effect. However, these weak stresses are *non-glide* stresses, which do not produce a driving force on the dislocations and thus should not affect the HD procedure (although they may influence the non-Schmid behaviour of bcc metals [28]). The MD time step was set to 1 fs. In order to maximize the effect of the MD acceleration, the temperature should be as low as possible, but specifically for Nb > 50–60 K, because the Arrhenius rate equation (Eq. (1)) is valid for Nb for $T \geq$ 50–60 K [4]. Therefore, the temperature was set equal to 75 K in the present simulations. In all MD runs under constant strain (described in Sec. 3.1), the dipole model was first equilibrated

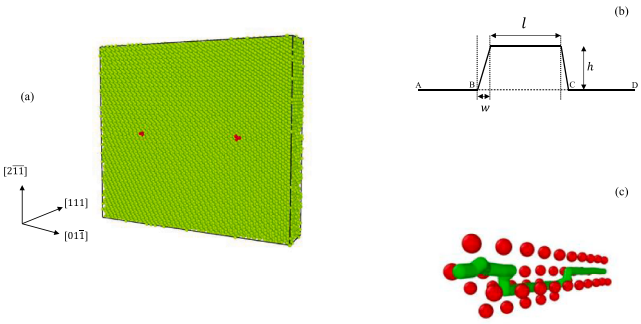

Fig. 1. (a) Atomistic configuration of the dipole model with two ½ [1 1 1](2 1 1) screw dislocations used in the MD simulations. The bcc atoms are marked green and the atoms in the dislocation cores are marked red, based on the coordination neighbour analysis implemented in the OVITO [41] program; (b) Sketch of a trapezoidal kink pair formed from an initially straight dislocation, denoted ABCD: w is the width of a single kink, l is the width of the KP, h is the height of the KP which is smaller or equal to the distance d between two Peierls valleys; (c) Snapshot of the atoms in one of the dislocation cores (in red) evidencing the formation of a kink-pair on the dislocation line (in green). (For interpretation of the references to colour in this figure legend, the reader is referred to the web version of this article.)

under a constant number of particles, pressure and temperature (*NPT* conditions) for 10 000 steps using the Nose-Hoover thermostat and at least 100 different initial velocity distributions. Temperature equilibration during the subsequent HD runs was achieved using a Langevin thermostat with a carefully chosen damping factor, so that the temperature of the mobile atoms varied only within ±1 K. The same seed for the Langevin thermostat was used in each HD run performed at every strain reduction level (see Sec. 3.1). The potential energy per atom varied within ±0.005 eV. All simulations were performed with LAMMPS [29] utilizing the embedded-atom method (EAM) potential of Farkas and Jones [30].

Static simulations were performed in order to obtain information on the energy barrier for the dislocation migration at 0 K under applied strain. The dipole model (see Fig. 1) was first equilibrated at 75 K and then strained at different strain reduction levels (see Sec. 3.1). In each case, the initial state represented 2 straight screw dislocations just *before* the first jump of one of them. The final state represented again 2 straight screw dislocations, with one of them *moved* to the next Peierls valley. The minimum energy path (MEP) under the applied strain from the initial to the final state through the transition state was determined using the nudged elastic band (NEB) method with improved tangent calculation [31]. Twelve replicas between the initial and the final state were constructed by linear interpolation. The calculations were performed with LAMMPS [29] using the FIRE minimization algorithm and a parallel NEB spring constant of 1.0 eV/Å^2. Convergence towards the MEP was rapidly achieved with force tolerance set to 0.001 eV/Å.

3. Methodology for accelerated molecular dynamics of dislocation mobility

3.1. Strain reduction

It is commonly accepted that at low temperatures, the movement of screw dislocations in bcc metals takes place by thermally- and stress-assisted nucleation of kink pairs (see Fig. 1b and c) [22] along the initially straight screw dislocation. A critical kink-pair (KP) is defined as a KP, for which the applied shear stress is sufficient to rapidly increase the KP *length l* (see Fig. 1b) after nucleation, leading to a jump of the dislocation to the next Peierls valley. For unstable (sub-critical) KPs, on the other hand, the attractive force between the formed kink and anti-kink predominates over the applied shear stress and they quickly annihilate. Different analytical models for the thermally-activated nucleation rate J_{kp} of critical KPs have been proposed in the literature at a constant temperature and shear stress τ, which can be written in the general form:

$$J_{\mathrm{kp}} = J_0 \exp\left(-\Delta G_{\mathrm{kp}}(\tau, T)/k_B T\right), \tag{3}$$

where $\Delta G_{\mathrm{kp}}(\tau, T)$ is the Gibbs energy of formation of a critical KP at a given constant shear stress τ and temperature T, and $J_0 = c\alpha(\tau, T)$, with c a material (or a fitting) constant and $\alpha(\tau, T)$ a function of T and/or τ, depending on the theoretical model used. The rate of KP nucleation is mainly controlled by the Gibbs energy of formation ΔG_{kp}.

Experimental studies on bcc Fe indicate that the KP entropy ΔS_{kp} is a small fraction of the total Gibbs energy ΔG_{kp} [32] and in most studies ΔG_{kp} is approximated by the enthalpy of KP formation ΔH_{kp}. The function $\alpha(\tau, T)$ is equal to $(\Delta H_{\mathrm{kp}}/k_B T)^{1/2}$ in the models of Celli et al. [33] as well as Büttiker and Landauer [34]; in the model of Hirth and Lothe [35] $\alpha(\tau, T) = (\tau/k_B T)$; in the models of Ackerman et al. [36] as well as Rodney and Proville [37] $\alpha(\tau, T) = (\beta/k_B T)^{1/2}$ where β is an adjustable parameter. In the case of small velocity damping at low temperatures, J_0 can be approximated by the result of transition state theory (TST), i.e., $J_0 = \nu_0$, where ν_0 is a characteristic attempt frequency of the system at the bottom of the potential well [38]. It can be seen that only in the TST case, the nucleation rate has a purely Arrhenius-type behaviour.

The enthalpy of KP formation ΔH_{kp} is commonly described by the phenomenological expression [39]:

$$\Delta H_{\mathrm{kp}}(\tau) = \Delta H_0 \left(1 - \left(\frac{\tau}{\tau_{\mathrm{c}}}\right)^m\right)^n, \tag{4}$$

where ΔH_0 is the enthalpy at zero stress, $0 < m \leq 1$ and $1 < n \leq 2$ are fitting parameters. Eq. (4) incorporates several published models for specific values of m and n [40].

The nucleation rate J_{kp} in Eq. (3) can be calculated from MD simulations as the inverse of the waiting time for the nucleation of a *critical* KP. The computation of the average waiting time at a given constant shear stress and temperature is the basis of our methodology to determine the stress and temperature dependence of $\Delta G_{\mathrm{kp}}(\tau, T)$ (including the entropy contribution ΔS_{kp}) by accelerated molecular dynamics (as described below). A similar approach was advocated in the study of dislocation nucleation from grain boundaries in Cu [24] under tensile stress.

A system in equilibrium, subjected to a constant strain γ, is described by the Helmholtz energy $F(\gamma, T)$. In the case of a constant stress ensemble, the system is described by the Gibbs energy. However, in standard MD shearing experiments performed at a constant strain rate, the strain increases *continuously* until the critical strain γ_{c} and the corresponding critical shear stress τ_{c} are reached. Under these conditions the driven system is *not* in mechanical equilibrium. In order to determine the average waiting time at *constant* shear strain γ and temperature T, we devise the following MD procedure.

The simulation supercell is first sheared with a computationally accessible strain rate (in our case $\dot{\gamma} = 1 \times 10^8\ \mathrm{s}^{-1}$) using *different* initial velocity distributions in order to determine the average critical strain $\overline{\gamma_{\mathrm{c}}}$ and average critical stress $\overline{\tau_{\mathrm{c}}}$. Afterward, a new simulation is started from the original configuration and the system is sheared again with the same strain rate, but now only until a *pre-defined*, reduced shear strain $\gamma_{\mathrm{red}} < \overline{\gamma_{\mathrm{c}}}$ [corresponding to a given strain reduction level (in %) $100(\overline{\gamma_{\mathrm{c}}} - \gamma_{\mathrm{red}})\ /\ \overline{\gamma_{\mathrm{c}}}$] is reached at a given MD time t_0 (see Fig. 2a). A linear elastic regime is observed up to the time t_0. Fit of τ as a function of strain in the elastic regime gives a shear modulus 46 ± 1 GPa, in excellent agreement with the value for the $G_{\{111\}}$ shear modulus, calculated with the elastic constants obtained with the EAM potential [30].

After the time t_0 has been reached, an MD run is performed at the constant shear strain γ_{red} until the time t_{jump}, which corresponds to the first jump of the screw dislocation (Fig. 2a). In each MD run, the first jump can be easily detected by the sudden small drop in the shear stress (see Fig. 2a). From t_{jump}, the waiting time $\Delta t_{\mathrm{w}} = t_{\mathrm{jump}} - t_0$ at constant strain is determined. The distribution of waiting times Δt_{w} and the average waiting time $\langle \Delta t_{\mathrm{w}} \rangle$ are then computed by sampling *different* initial velocity distributions. The average waiting time $\langle \Delta t_{\mathrm{w}} \rangle$ for the first jump increases rapidly with increasing strain reduction (see Fig. 2b) and clearly indicates the necessity for an accelerated molecular dynamics treatment, if higher strain reduction levels are targeted at.

It should be noted that the shear stress remains practically constant during these MD runs (with variations in a very narrow range of ±0.003 GPa for our system, see Fig. 2), so that the system can be regarded as subjected to a constant shear stress as well. This procedure allows, first of all, to study, in principle, the nucleation of both unstable and critical KPs at *lower* stress levels $\tau < \overline{\tau_{\mathrm{c}}}$. Further, the nucleation of KPs at constant shear stress τ and temperature T becomes a *statistical* (probabilistic) event driven *mainly* by thermal vibrations, which is a key prerequisite for the subsequent application of hyperdynamics.

Detailed atomistic analysis of the MD configurations using the coordination neighbour analysis (CNA), implemented in the OVITO program [41], shows that the first jump takes place by nucleation and growth of a kink pair on one of the screw dislocations, in which each of the two kinks are along 2 different (1 1 0) slip planes (see Fig. 1c). The first jump occurs statistically evenly-distributed on the left and the right

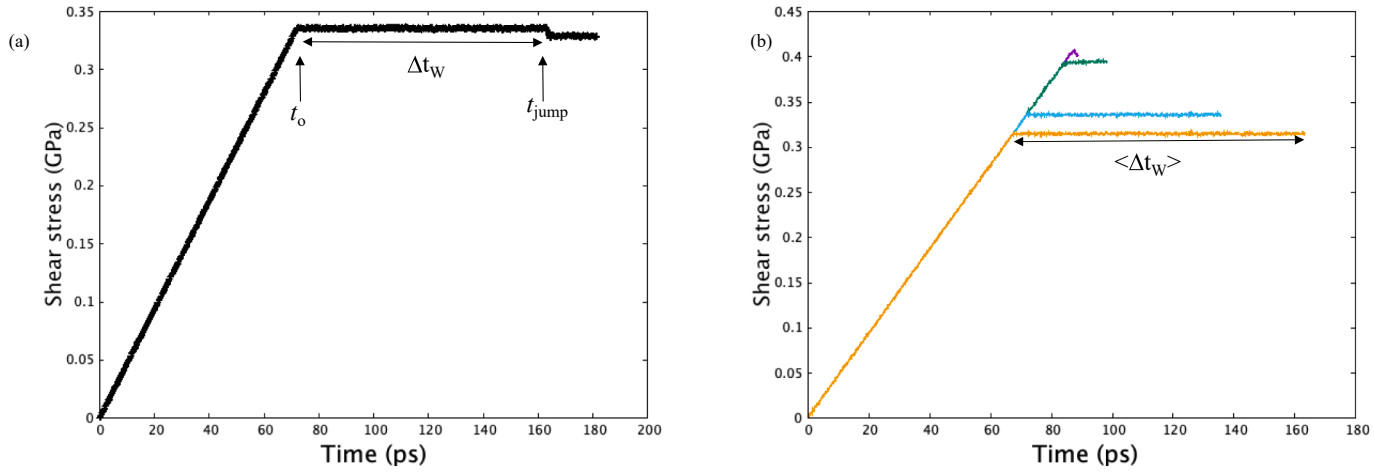

Fig. 2. (a) A typical stress-time curve at 20% strain reduction ($\tau = 0.33$ GPa). The time t_0 marks the start of the constant strain regime, t_{jump} marks the first jump and $\Delta t_w = t_{jump} - t_0$; (b) Stress-time curves at 75 K for standard shearing (pink) and constant strain reduction: 5 % (green), 20% (blue) and 25% (orange). The average waiting times $\langle \Delta t_w \rangle$ in Fig. 2b are 12, 57 and 95 ps, respectively. (For interpretation of the references to colour in this figure legend, the reader is referred to the web version of this article.)

screw dislocation of our dipole model.

3.2. Bond-boost potential

In the HD method, acceleration is achieved by adding a boost potential ΔV_b to the original interatomic potential [18]. In this way, the system can escape faster from a given local minimum, because the biased potential $V + \Delta V_b$ is shallower than the potential well in the original potential energy surface V. The boost potential ΔV_b is generally a function of the instantaneous coordinates of the boosted atoms. The boost factor (BF) is defined at a given MD step t_i by [18]:

$$\mathrm{BF}_i = \exp\left(\frac{\Delta V_b(t_i)}{k_B T}\right) \tag{5}$$

The accelerated time of the hyperdynamics (t_{hyp}) is given by [18]:

$$t_{hyp} = \Delta t_{MD} \sum \mathrm{BF}_i, \tag{6}$$

where the sum is over the performed MD integration steps and Δt_{MD} is the MD integration time step.

The migration of a screw dislocation from one Peierls valley to another via the formation of KPs is a complex, collective event and different collective variables (CV) can be, in principle, designed to describe quantitatively the transition. Within our method, we use a modification of the bond-boost scheme [20], which is validated below. In this boost potential, the CV is the maximum relative change of the bonds in the boosted region. At every MD time step during boosting ΔV_b is defined as:

$$\Delta V_b = \begin{cases} V_{max}\left[1 - \dfrac{\varepsilon_{max}}{q}\right]^2 & \text{if} \quad \varepsilon_{max} < q \\ 0, & \text{if} \quad \varepsilon_{max} \geq q \end{cases} \tag{7}$$

as implemented in LAMMPS [29]. V_{max} is the magnitude of the boost potential, ε_{max} is the *maximum* bond strain at a given MD step ($\varepsilon_{max} = \max_\alpha\{\varepsilon_\alpha\}$), where $\varepsilon_\alpha = \|b_\alpha - b_\alpha^0\|/b_\alpha^0$, b_α is the instantaneous value of bond α, b_α^0 is the initial value of bond α in the boosted region and q is the so-called *threshold* parameter. The achievable boost factor depends both on q and V_{max}.

The boost potential reaches its maximum value (V_{max}) when the bonds are at equilibrium (i.e., when $\varepsilon_{max} = 0$) and this leads to a maximum boost factor $\mathrm{BF}_{max} = \exp\left(\frac{V_{max}}{k_B T}\right)$. On the other hand, the boost potential goes to zero when the fractional change in bond length ε_{max} reaches the threshold value q. Eq. (7) guarantees [19] that the boost potential satisfies the condition $\Delta V_b = 0$ at any dividing hypersurface between two local minima (at the transition state), one of the main requirements of the HD method [18]. In this case the boost factor becomes equal to 1 and there is no boosting.

At each MD step the bond with the maximum bond strain ε_{max} is first determined, then the *extra* force on this bond $\delta \boldsymbol{F}_b$ is calculated [19], after which equal and opposite forces $\pm$½ $\delta \boldsymbol{F}_b$ are applied *along* the bond direction to the two atoms forming the bond. Here a bond is defined simply as any interatomic distance smaller or equal to a cut-off distance of 3.25 Å, taken between the first and the second nearest-neighbour distances. This cut-off radius ensures that the boost potential is *short-ranged* and should not be affected (in first approximation) by the long-range elastic interactions between the two dislocations along the Z axis.

To summarize, the application of the HD method for the acceleration of the dislocation mobility within the here proposed method is based on the following assumptions: (i) The system remains in thermal equilibrium at a given strain γ and temperature T, which is realised with our strain reduction procedure, (ii) the local minima represent neighbouring Peierls valleys, occupied by a *straight* screw dislocation before and after the transition; (iii) the transition state between the two local minima represents the *nucleation of critical KPs,* which is confirmed by dislocation analysis using OVITO [41]; (iv) the KP formation is accompanied by a *significant* change of the lengths of selected nearest-neighbour bonds between atoms in the dislocation core, such that the boost potential (Eq. (7)) with physically meaningful threshold parameters V_{max} and q can be operational.

In order to validate these assumptions and to determine optimal values for the potential parameters V_{max} and q, *unboosted* constant-strain MD runs were first performed at 75 K as introduced in the previous subsection. The first jump of the screw dislocation in the unboosted constant-strain MD simulations was monitored by the variation of the maximum bond strain (ε_{max}) and the maximum shift (ΔR_{max}) of the atoms in the dislocation core with MD time. ΔR_{max} is defined as the maximum atomic shift at a given MD step calculated for all atoms in the dislocation cores, with respect to their initial positions. Both parameters exhibit fluctuations for times $t < 122$ ps and a sharp jump of the average values $\langle \varepsilon_{max} \rangle$ and $\langle \Delta R_{max} \rangle$ at $t_{jump} \sim 122$ ps at 20% strain reduction (see Fig. 3). Such a behaviour is qualitatively similar for *all* strain-reduction levels.

Visualization of the topology of the screw dislocations with time using the OVITO [41] program shows that the maxima in ε_{max} ($\varepsilon_{max} > 0.1$

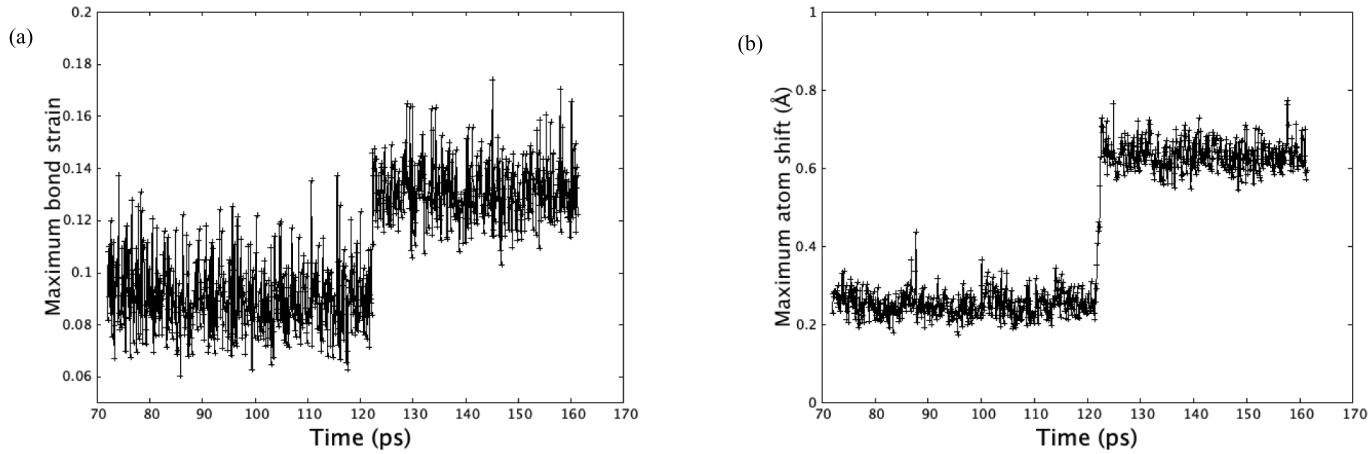

Fig. 3. Variation with time of the maximum bond strain ε_{max} (a) and the maximum atomic shift ΔR_{max} of the atoms in the dislocation cores (b); data for 20% strain reduction.

for our setup) for times $t < 122$ ps correspond to the nucleation of *unstable* KPs, while the large jumps of ΔR_{max} and ε_{max} at about 122 ps correspond to the nucleation of a *critical* KP on *one* of the screw dislocations and a subsequent jump (within ~1 ps) of the corresponding screw dislocation. This *correlation* between ΔR_{max}, as well as ε_{max}, and the topology of the screw dislocations shows that by monitoring ΔR_{max} and ε_{max} it is possible to detect correctly the transition state. Further, this finding suggests that the selected CV and the form of the bond-boost potential (Eq. (7)) should be suitable for acceleration of the screw dislocation.

3.3. Hyperdynamics runs

After a given reduced strain γ_{red} is reached within the strain reduction approach (Sec. 3.1), a constant temperature and constant strain HD run is performed using the bond-boost potential (Sec. 3.2, Eq. (7)). The boosted region consists of all atoms in the dislocation cores of the two screw dislocations (e.g., all atoms at a distance less than 3.9 Å from the corresponding straight dislocation line, as validated with the OVITO [41] program). The maximum atomic shift ΔR_{max} within the boosted region is monitored at every MD step. If ΔR_{max} becomes larger than the threshold value 0.55 Å (see above), the HD run is aborted and the results are analysed. The extra computational cost for the HD generally scales as the number of atoms in the boosted region, but in our case the number of atoms in the dislocation cores is very small (240 atoms), so that the computational overhead is negligible.

3.4. Determination of the optimum bond-boost potential parameters

Increase of ε_{max} on a short time scale (~1 ps) indicates that the system is approaching a transition state. Selecting a too low threshold value (q smaller than the average ε_{max} value *between* unstable KP nucleation events, in our case ~0.085), the boosting will stop (ΔV_b will become zero) prematurely. During an MD run, it is not known *a priori* if a nucleated KP will be a critical or unstable KP. Thus, selecting a too-high threshold value ($q > 0.11$), on the other hand, could lead to over-boosting. The boost potential will be too strong and will not go to zero, although the screw dislocation will already be (almost) entirely in the next Peierls valley. The threshold parameter was set tentatively equal to 0.09 and this value will be confirmed further below.

The parameter V_{max} in Eq. (7) determines the maximum achievable boost for a fixed q parameter. Ideally, V_{max} should be as high as possible to give a significant acceleration through Eqs. (5) and (6). However, it should be not too high, so that the boost potential does not create additional potential barriers and/or does not change strongly the shape of the original potential basins. For a *properly selected* V_{max}, the following conditions should be fulfilled: (i) acceleration of the KP nucleation rate, manifested by the decrease of the average waiting time during boosting $\langle \Delta t_w^b \rangle$ as well as a decrease of $\langle \Delta t_w^b \rangle$ with increasing V_{max}; (ii) the actual time evolved during the HD run, $\langle t_{hyp} \rangle$, remains equal to the average waiting time *without* boosting, $\langle t_{hyp} \rangle = \langle \Delta t_w \rangle$.

The V_{max} parameter was first increased in steps from 0 to 0.1 eV for 20 % strain reduction (see Fig. 4). Up to $V_{max} \sim 0.03$ eV, $\langle \Delta t_w^b \rangle$ decreases, whereas $\langle t_{hyp} \rangle$ remains, with increasing V_{max}, constant and equal (within error limits) to the value of $\langle \Delta t_w \rangle$ at $V_{max} = 0.0$, as expected. This emphasizes the fact that up to $V_{max} \sim 0.03$ eV our boost model works correctly, without modifying significantly the transformation pathway for the onset of dislocation migration. Above $V_{max} \sim 0.03$ eV, $\langle t_{hyp} \rangle$ increases rapidly.

As a further validation, the waiting times with and without boosting were compared at 5, 20 and 25 % strain reduction levels with V_{max} set equal to $4k_BT$ (~0.025 eV) for two threshold values. The various average times, obtained from these HD runs, are summarized in Table 1. The decrease of the shear stress with increasing strain reduction leads to an increase of the average waiting time without boosting $\langle \Delta t_w \rangle$. The HD runs lead for all strain reduction levels to acceleration (a decrease of the boosted waiting time $\langle \Delta t_w^b \rangle$, compared to $\langle \Delta t_w \rangle$) and the condition $\langle t_{hyp} \rangle = \langle \Delta t_w \rangle$ is fulfilled well within error limits for the threshold $q = 0.09$. For larger thresholds, e.g. $q = 0.12$, $\langle \Delta t_w^b \rangle$ decreases further only marginally, but the average hypertimes become unphysically high, as can be inferred already from Fig. 3a. Based on this analysis, V_{max} and q were set equal to 0.025 eV and 0.09 in the subsequent HD simulations at higher strain reduction levels. In the case of adatom surface diffusion, the boost potential is considered independent of temperature (see e.g. Refs. [19,42]). In the present case, the nucleation of critical KPs is generally stress- as well as temperature-dependent [9,22,40]. This would require eventually optimization of the bond-boost parameters at different temperatures in order to comply with the requirement $\langle t_{hyp} \rangle = \langle \Delta t_w \rangle$.

The average hypertime $\langle t_{hyp} \rangle$ increases linearly with increasing $\langle \Delta t_w^b \rangle$, indicating that the bias potential is properly selected and the average boost factor $\langle BF \rangle = 1.9 \pm 0.1$ is well sampled. This was further checked by plotting the individual hypertimes versus the boosted waiting times for the different strain reduction levels. All HD runs with $q = 0.09$ show little scatter (see examples in Fig. 5), while $q = 0.12$ leads to a much larger scatter, indicating again that the boost potential with $q = 0.09$ and $V_{max} = 0.025$ eV is properly selected [42].

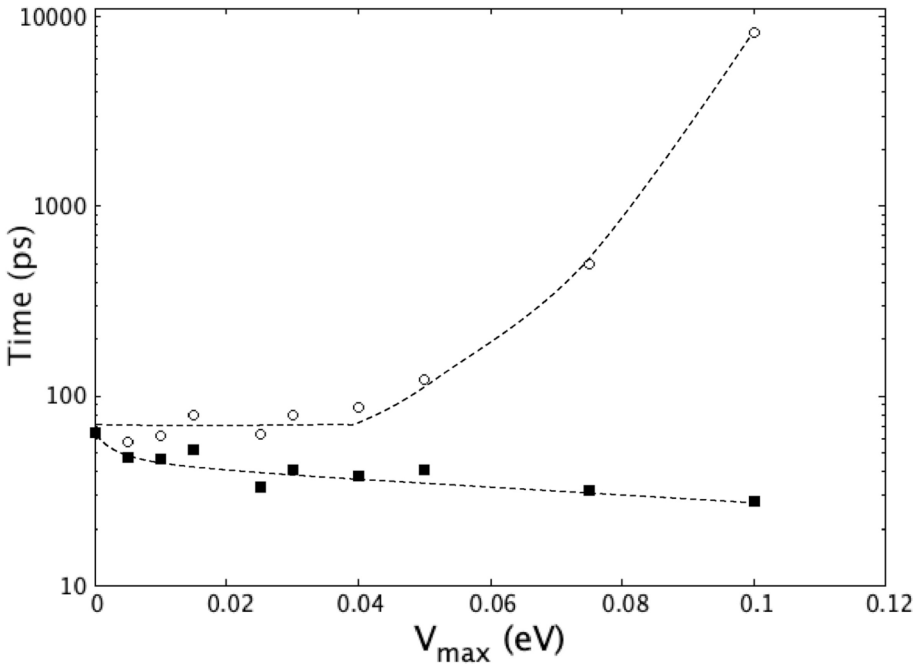

Fig. 4. Variation of the boosted waiting time (full squares) and the hypertime (empty circles) with increasing V_{max} parameter. The dashed lines are only a guide for the eye.

Table 1
Average waiting time without boosting $\langle \Delta t_w \rangle$, average boosted waiting time $\langle \Delta t_w^b \rangle$ and average hypertime $\langle t_{hyp} \rangle$ (all in ps) together with their estimated standard deviations for different shear stresses τ and threshold parameters q.

Strain Reduction	τ(GPa)	q	$\langle \Delta t_w^b \rangle$	$\langle t_{hyp} \rangle$	$\langle \Delta t_w \rangle$
5%	0.39	0.09	8 ± 7	16 ± 15	12 ± 12
		0.12	7 ± 6	45 ± 45	
20%	0.33	0.09	32 ± 36	60 ± 68	57 ± 50
		0.12	30 ± 25	207 ± 188	
25%	0.31	0.09	60 ± 60	113 ± 120	95 ± 86
		0.12	55 ± 50	393 ± 374	

4. Results and discussion

4.1. Distribution of hypertimes

For our simulation setup, the average critical time $\overline{t_c}$ and the average critical shear stress $\overline{\tau_c}$ at 75 K, obtained from standard MD simulations using a typical strain rate of $1x10^8$ s^{-1}, are 91 ± 5 ps and 0.41 ± 0.02 GPa, respectively. Experimentally, the CRSS τ^* for Nb at 75 K, measured at a shear strain rate of $1.5x10^{-4}$ s^{-1}, is almost 50% smaller – approximately 0.23 GPa [4]. The critical time $\overline{t_c}$ increases almost exponentially with decreasing strain rate (see Fig. 6). Therefore, trying to determine $\overline{t_c}$ with a strain rate of 1.5×10^{-4} s^{-1} using standard MD simulations would require infeasibly long simulation times, e.g., 4320 years on a 3 GHz Intel i5 Processor with 6 cores. Instead, we can apply the here proposed methodology.

We thus increased systematically the strain reduction from 20 to 50 %, performing at each strain level *at least* 100 HD runs, using the bond-boost potential (Eq. (7)) with parameters $V_{max} = 0.025$ eV and $q = 0.09$. The *onset* of the screw dislocation migration via the nucleation of a critical KP was observed in *all* HD runs at *all* constant stress levels down to 0.21 GPa. This demonstrates that the onset of the screw dislocation mobility can be realized at *lower* shear stresses with this procedure.

At constant shear stress and temperature, the nucleation of critical KPs can be regarded as a random process driven only by thermal fluctuations of the dislocation cores. This probabilistic behaviour leads

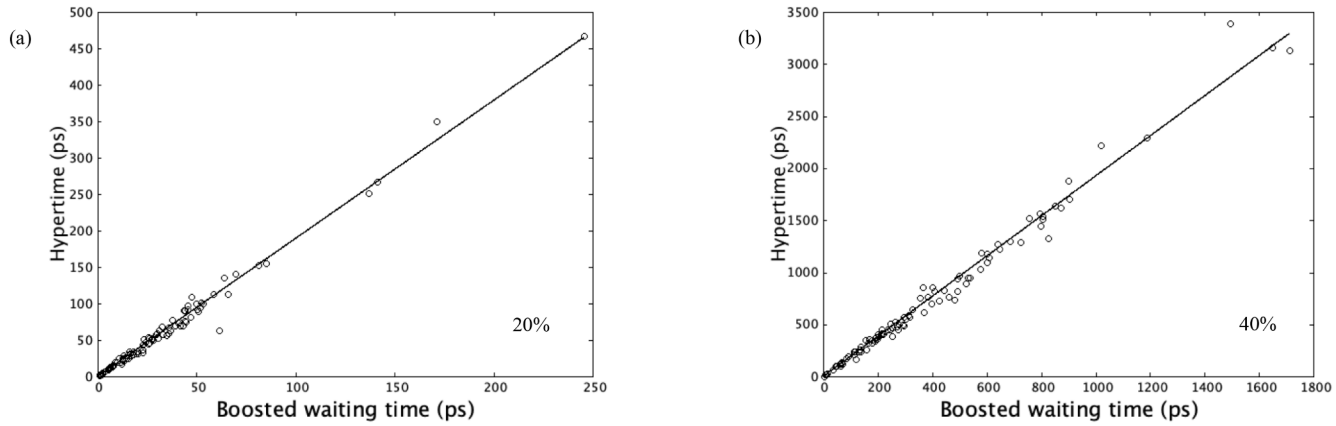

Fig. 5. Hypertimes (o), as defined in Eq. (6), versus the boosted waiting time for: (a) 20% and (b) 40% strain reduction. The full lines are linear fits through the data points in each panel, yielding average boost factors equal to 1.9 ± 0.1.

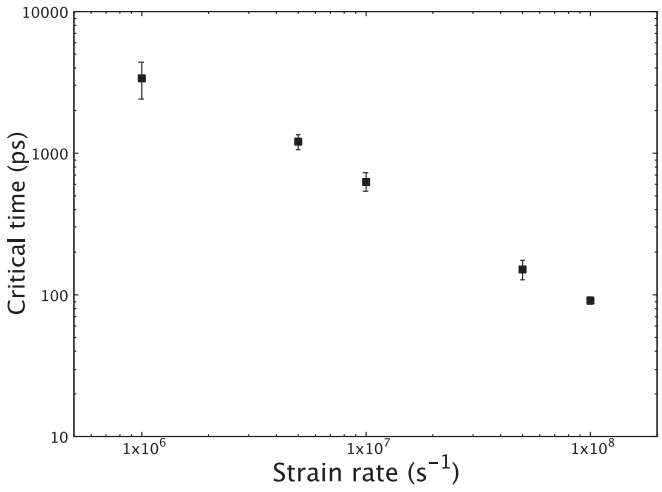

Fig. 6. Variation of the average critical time $\bar{t_c}$ with strain rate.

naturally to a distribution of the waiting times. The AMD method allows to determine the distribution of the hypertimes and to calculate the average hypertimes $\langle t_{hyp}\rangle$ over a *larger* time scale.

If the probability of nucleation of critical KPs in any given time interval is constant and the nucleation of a given KP is independent of any previous nucleation, the probability distribution of forming p critical KPs can be considered as a general Poisson process:

$$P(t,p) = \frac{(J_{kp}t)^p}{p!}\exp(-J_{kp}t), \tag{8}$$

in which the nucleation rate of critical KPs J_{kp} should be *independent* of time. In principle, Eq. (8) can be used to fit the distributions obtained from the HD runs, and thus determine the nucleation rates J_{kp}.

The distribution of the hypertimes, obtained from the present HD runs (see example in Fig. 7), exhibits statistical scatter and qualitatively resembles the Poisson distribution with $p = 2$ (formation of 2 KPs on top of each other). This is a strong indication that the nucleation of critical KPs is a statistically random event, one of the key assumptions of HD. However, the shape of the distributions is actually more right-skewed than the Poisson distribution, the maximum values of the distributions and the estimated standard deviations $\sigma(\langle t_{hyp}\rangle)$ increase with increasing strain reduction level, respectively with decreasing shear stress (see Table 1). The enthalpy of formation of critical KPs increases at lower

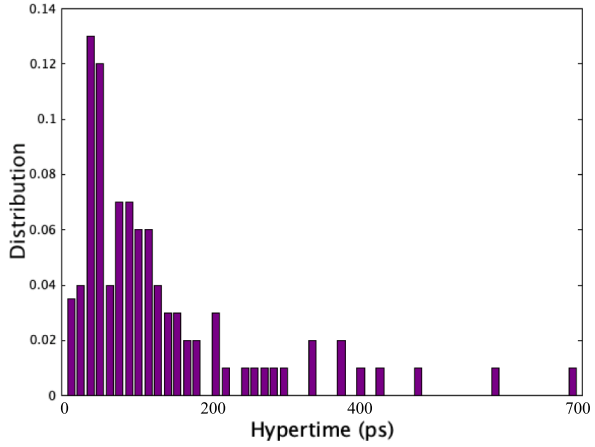

Fig. 7. Distribution of the hypertimes at 25% strain reduction.

stresses (see Eq. (4) and Sec. 4.2). This leads to a spread of the hypertime distribution, because statistically larger hypertimes are necessary to overcome the higher potential barriers at lower stresses. A detailed analysis of the hypertime distributions will be the subject of a future study.

4.2. Determination of the activation Gibbs energy for kink-pair formation

The average nucleation rate of the critical KPs can be determined from the HD runs, without fitting Eq. (8) to the hypertime distributions, as:

$$\langle J_{kp}\rangle = 1/\langle t_{hyp}\rangle. \tag{9}$$

The nucleation rates, calculated from Eq. (9), decrease with increasing strain reduction (decreasing shear stress, respectively). The average nucleation rate $\langle J_{kp}\rangle$ allows, in turn, to determine the average Gibbs energy for KP formation, using Eq. (3). However, it is necessary to estimate J_0 in Eq. (3). For that purpose, we take into account that at $\tau = \overline{\tau_c}$ the Gibbs energy of kink-pair formation $\Delta G_{kp} \approx \Delta H_{kp}$ should be zero (see Eq. (4)) and thus $J_{kp} = J_0$ at $\tau = \overline{\tau_c}$. But at $\tau = \overline{\tau_c}$, $\langle t_{hyp}\rangle$ is zero and the nucleation rate is determined mainly by the variation of the average critical waiting time $\overline{t_c}$. Thus, we propose that:

$$J_0 = 1/\sigma(\bar{t}_c), \tag{10}$$

where $\sigma(\bar{t_c})$ is the estimated standard deviation of the average critical time $\bar{t_c}$, obtained from the MD simulations at constant strain rate (see Sec. 3.1). Combining Eq. (3), (9) and (10), $\langle \Delta G_{kp}\rangle$ is given by:

$$\langle \Delta G_{kp}\rangle = -k_B T \ln\left[\frac{\sigma(\bar{t_c})}{\langle t_{hyp}\rangle}\right] \tag{11}$$

Since both $\sigma(\bar{t_c})$ and $\langle t_{hyp}\rangle$ depend generally on stress and temperature, Eq. (11) allows to calculate $\langle \Delta G_{kp}\rangle$ without assuming *specific* stress- and/or temperature dependence of the pre-Arrhenius factor J_0 in Eq. (3), as in Refs. [34–36], or performing additional free-end nudged elastic band calculations in order to determine the attempt frequency ν_0, as in Refs. [23,24,43], provided that the boost potential fulfils the requirement $\langle t_{hyp}\rangle = \langle \Delta t_w\rangle$.

Thus, the AMD methodology introduced in this work, allows us to compute *directly* the stress and temperature-dependent Gibbs energy surface $\Delta G_{kp}(\tau, T)$ of thermally-activated kink-pair formation. Fig. 8 shows an example of the stress-dependence of $\Delta G_{kp}(\tau, T)$ for a screw dislocation in bcc Nb at a temperature of $T = 75$ K, determined at several stress levels.

From Fig. 8, it can be seen *a posteriori* that the maximum of the boost potential $V_{max} = 0.025$ eV used in our HD implementation, is *similar* to the values of ΔG_{kp}. This agrees well with the general requirement that the boost potential should be comparable to the natural energy barriers of the system under study [19]. The $\langle \Delta G_{kp}\rangle$ values are in good agreement with Eq. (4) with adjusted parameters $m = 0.5 \pm 0.2$, $n = 1.0 \pm 0.1$ and $\Delta H_0 = 0.14 \pm 0.06$ eV.

0 K minimum energy paths $\Delta E(\tau, \alpha)$ as a function of the reaction coordinate α and at different shear stresses τ were calculated with the NEB method [31] (i.e., *no* boosting included) and are shown in Fig. 9. To facilitate comparison, the energies are referenced with respect to the initial structure, i.e., $\Delta E(\tau, \alpha) = E(\tau, \alpha) - E(\tau, 0)$, where $E(\tau, \alpha)$ is the total energy at a specific reaction coordinate value α and $E(\tau, 0)$ is the total energy of the initial configuration. The energy maxima (barriers) $\Delta E(\tau)_{max}$ decrease and move toward smaller α values with increasing the applied stress, in agreement with previous NEB calculations under applied stress [44–46]. Visualization with OVITO [41] of the atomic configurations, as generated with the NEB method (not displayed here explicitly), clearly shows that the transition state is associated with the

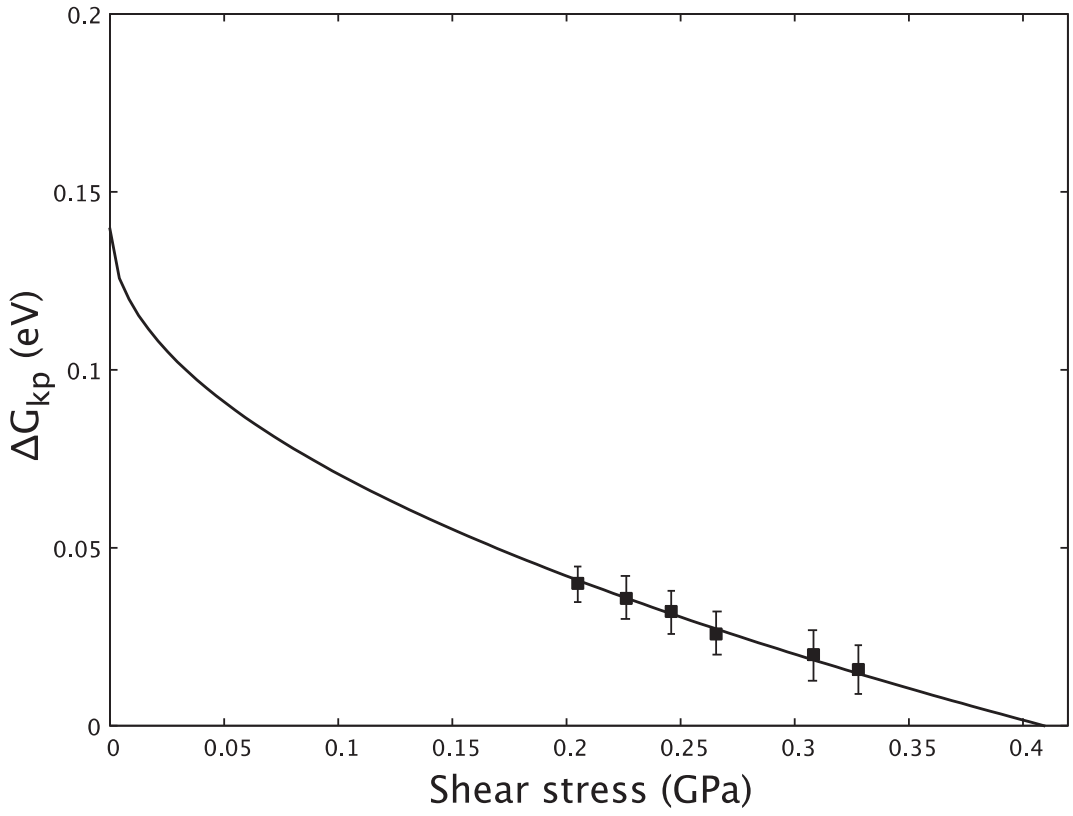

Fig. 8. Average Gibbs energies (■) for kink-pair formation at 75 K as a function of shear stress, determined from Eq. (11). The full line is a fit using Eq. (4).

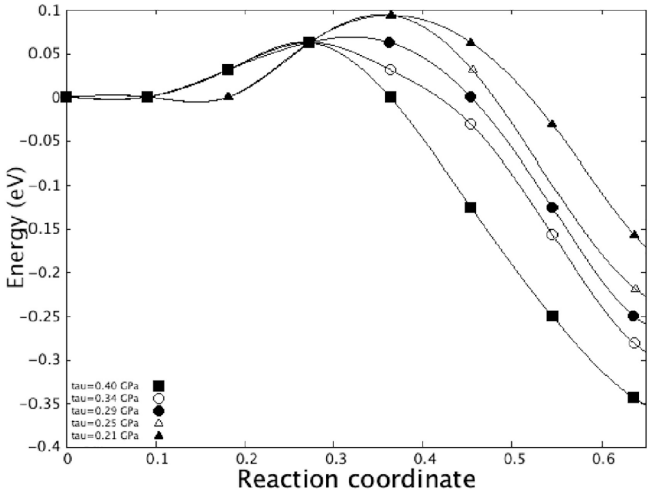

Fig. 9. Minimum energy paths for migration of the screw dislocation at different stress levels, calculated using the NEB method without boosting at 0 K. Only the most relevant first part of the paths, which contains the energy barriers corresponding to the activated (transition) state, is shown. The lines are only a guide for the eye.

nucleation and growth of a kink-pair. Moreover, the width l of the critical KPs (see Fig. 1c) of about 3.0 Å, as observed in the NEB simulations, is practically the same as the width of the critical KPs documented during the AMD simulations.

In order to estimate the enthalpies of KP nucleation from the NEB calculations, the $\Delta E(\tau)_{\max}$ values have to be corrected for the work, $W(\tau)$, done by the applied stress: $\Delta H_{\mathrm{NEB}}(\tau) = \Delta E(\tau)_{\max} - W(\tau)$ [46]. The external work $W(\tau)$ is approximately taken equal to τb^3. The calculated values $\Delta H_{\mathrm{NEB}}(\tau)$ decrease from 0.064 eV to 0.0045 eV with increasing stress from 0.21 to 0.40 GPa. The relatively good agreement between these enthalpies, obtained at 0 K and without boosting, and the $\langle \Delta G_{\mathrm{kp}} \rangle$ values, obtained at 75 K and with the AMD procedure (see Fig. 8), indicates that the activated (transition) state is neither (strongly) affected by the entropic contribution nor by the application of the boost potential. The consistency of the static and dynamic calculations provides a further validation of the proposed methodology.

The activation volume of dislocation migration is thermodynamically defined as the derivative of the Gibbs energy with respect to stress:

$$V^* = -\partial \langle \Delta G_{\mathrm{kp}} \rangle / \partial \tau. \tag{12a}$$

In the present method, V^* can be calculated directly using Eq. (12a), without performing simulations at different strain rates and using the expression $V^* = k_B T \Delta \ln(\dot{\gamma}) / \Delta \tau$ [4]. For example, we obtain $V^* = 0.02 \pm 0.01\ b^3$ at $\tau = 0.23$ GPa. These values are much smaller than the experimental values ($4\ b^3$), reported for Nb by Takeuchi et al. [4].

We stress that these low activation volumes are not caused by the application of the AMD method. The same too low activation volumes are also obtained using brute force MD simulations. The possible reasons for the differences between simulations and experiments are: (1) in real crystals, in comparison with the present MD simulations, there are always vacancies, impurities and forest dislocations which affect strongly the flow properties of bcc metals and lead to much larger activation volumes and enthalpies of KP formation; (2) the interatomic interactions as provided by the EAM potential are not sufficiently well reproducing the true interactions. As for the second point, the recent, very successful advancements in developing machine learning potentials (see, e.g., Refs. [47,48,49]) may offer future solutions, also in combination with the present AMD technique.

Specifically, according to Conrad [50], the activation volume can be written phenomenologically as:

$$V^* = b d^* l^*, \tag{12b}$$

where d^* is the distance swept by the dislocation during the jump from one to the next Peierls valley (equal to $2b\frac{\sqrt{2}}{3}$ for KPs on the (1 1 0) slip plane) and l^* is the activation length. Apparently, l^* is much larger in real crystals. The formation of isolated kinks and KPs requires an abrupt change of the topology of the initially straight dislocation and l^* can be tentatively identified as the width w of the kinks, see Fig. 1b. Both in our standard MD and AMD simulations, w is 0.2Å. By increasing the length L_y of the simulation supercell from $10b$ to $40b$, it was confirmed that the width of the isolated kink remains practically the same and does not depend on L_y. Using the above value for w, Eq. (12b) leads to $V^* = 0.07\,b^3$. This estimate is of the same order as the calculated activation volume, using Eq. (12a). The absence of any defects in the simulation supercell, apart from the dislocation itself, apparently leads to a small width of the KPs and low activation volumes.

Finally, in order to estimate the accessible strain rate reduction with the presented methodology, we assume that the activation free energy for dislocation motion ΔG is, in a first approximation, equal to the average Gibbs energy of KP formation $\langle \Delta G_{\mathrm{kp}} \rangle$ [39,51]:

$$\Delta G(\tau) \approx \langle \Delta G_{\mathrm{kp}}(\tau, T) \rangle. \tag{13a}$$

In this case, it follows from Eq. (1) and (3) that:

$$\ln\left(\frac{\dot{\gamma}}{\dot{\gamma}_0}\right) \approx \ln\left(\frac{\langle J_{\mathrm{kp}} \rangle}{J_0}\right) = -\langle \Delta G_{\mathrm{kp}}(\tau, T) \rangle \Big/ k_B T. \tag{13b}$$

Since $\langle \Delta G_{\mathrm{kp}} \rangle$ increases with decreasing shear stress τ (see Eq. (4) and Fig. 8), Eq. (13b) shows that *lower* strain rates $(\dot{\gamma}/\dot{\gamma}_o)$ (i.e., more negative values for the right side of Eq. (13b)) can be achieved with accelerated MD simulations, *if* nucleation of critical KPs and the subsequent start of screw dislocation motion can be *realized* at *lower stresses*, as has been demonstrated above.

5. Conclusions and outlook

A methodology for the study of the *onset* of dislocation mobility at constant temperature and constant strain has been introduced. Our method features a strain reduction procedure, which enables the coupling to accelerated molecular dynamics (AMD) using the hyper-dynamics method and the bond-boost potential.

It has been demonstrated, on the example of bcc Nb, that the developed AMD technique:

(i) can successfully be applied to complex metal systems like models with screw dislocations, in which the temperature- and stress-driven transition from one state to another involves cooperative motion of a relatively large number of atoms (nucleation of kink pairs);

(ii) can access l*ower* shear stresses, *comparable* to the CRSS, typically measured in macroscopic deformation experiments;

(iii) gives direct access to the stress- and temperature-dependent Gibbs energy surface $\Delta G_{\mathrm{kp}}(\tau, T)$ of thermally-activated kink-pair formation from finite-temperature MD simulations.

The calculation of the Gibbs energy does not require any additional assumptions except that the double-kink formation mechanism is a thermally-activated process. By standard thermodynamic relations this enables the determination of the corresponding activation enthalpy, entropy and volume.

The present approach can be straightforwardly implemented using existing molecular dynamics codes like LAMMPS. It is not limited to simulation models containing only 2 screw dislocations, bcc Nb or the employed EAM potential. The method can be extended to mixed dislocations, other metals and different interatomic potentials, e.g. machine-learning potentials, because the calculation of the boost potential does not depend explicitly on the form of the underlying interatomic potential. The method can be applied as well to other stress-driven processes like dislocation drag by impurities or dislocation mobility in multi-component alloys.

CRediT authorship contribution statement

Blazej Grabowski: Conceptualization, Methodology, Funding acquisition, Project administration. **Nikolay Zotov:** Investigation, Formal analysis, Visualization, Software, Writing – original draft.

Declaration of Competing Interest

The authors declare that they have no known competing financial interests or personal relationships that could have appeared to influence the work reported in this paper.

Acknowledgements

This project has received funding from the European Research Council (ERC) under the European Union's Horizon 2020 research and innovation programme (grant agreement Nos. 639211 and 865855).

References

[1] E. Orowan, Fracture and strength of solids, Rep. Prog. Phys. 12 (1948) 183–230.
[2] G. Taylor, Thermally-activated deformation of bcc metals and alloys, Prog. Mater Sci. 36 (1992) 29–61.
[3] T. Suzuki, Y. Kamimura, H.O.K. Kirchner, Plastic homology of bcc metals, Phil. Mag. A 79 (7) (1999) 1629–1642.
[4] S. Takeuchi, T. Hashimoto, K. Maeda, Plastic deformation of bcc metal single crystals at very low temperatures, Trans. Japan Inst Metals 23 (1982) 60–69.
[5] R. LeSar, Simulations of dislocation structure and response, Ann. Review Cond. Matter Phys. 5 (1) (2014) 375–407.
[6] Z.S. Basinski, M.S. Duesbery, R. Taylor, Influence of shear stress on screw dislocations in a model sodium lattice, Can. J. Phys. 49 (16) (1971) 2160–2180.
[7] D.E. Segall, A. Strachan, W.A. Goddard III, S. Ismail-Beigi, T.A. Arias, Ab initio and finite-temperature molecular dynamics studies of lattice resistance in tantalum, Phys. Rev. B 68 (2003), 014104.
[8] C. Domain, G. Monnet, Simulation of screw dislocation motion in iron by molecular dynamics simulations, Phys. Rev. Lett. 95 (2005), 215506.
[9] M.R. Gilbert, S. Queyreau, J. Marian, Stress and temperature dependence of screw dislocation mobility in α-Fe by molecular dynamics, Phys. Rev. B 84 (2011), 174103.
[10] L. Proville, D. Rodney, M.-C. Marinica, Quantum effect on thermally activated glide of dislocations, Nature Materials 11 (10) (2012) 845–849.
[11] S.L. Frederiksen, K.W. Jacobsen, Density functional theory study of screw dislocation core structures in bcc metals, Phil. Mag. 83 (2003) 365–375.
[12] L. Dezerald, L. Ventelon, E. Clouet, C. Denoual, D. Rodney, F. Willaime, Ab initio modelling of the two-dimensional energy landscape of screw dislocations in bcc transition metals, Phys. Rev. B 89 (2014), 024104.
[13] R. Gröger, V. Vitek, Explanation of the discrepancy between the measured and atomistically calculated yield stresses in body-centred cubic metals, Phil. Mag. Lett. 87 (2) (2007) 113–120.
[14] A. Seeger, U. Holzwarth†, Slip planes and kink properties of screw dislocations in high-purity niobium, Phil. Mag. 86 (25-26) (2006) 3861–3892.
[15] G. Testa, N. Bonora, A. Ruggiero, G. Iannitti, Flow stress of bcc metals over a wide range of temperature and strain rates, Metals 10 (2020) 120–130.
[16] S. Nemat-Nasser, W. Guo, Flow stress of commercially pure niobium over a broad range of temperatures and strain rates, Mater. Sci. Eng. A 284 (1-2) (2000) 202–210.
[17] R.J. Zamora, D. Perez, E. Martinez, B.P. Uberuaga, A.F. Voter, Accelerated molecular dynamics methods in a massively parallel world, in: W. Andreoni, S. Yip (Eds.), Handbook of Materials Modelling, Springer International Publishing, 2018.
[18] A.F. Voter, A method for accelerating the molecular dynamics simulation of infrequent events, J. Chem. Phys. 106 (11) (1997) 4665–4677.
[19] R.A. Miron, K.A. Fichthorn, Accelerated molecular dynamics with the bond-boost method, J. Chem. Phys. 119 (12) (2003) 6210–6216.
[20] S.Y. Kim, D. Perez, A.F. Voter, Local hyperdynamics, J. Chem. Phys. 139 (14) (2013) 144110.
[21] E.V. Duda, G.V. Kornich, On the construction of a bias potential for atomic system simulation by the hyperdynamics method, J. Surface Investig.: X-ray, Synchrotron Neutron Tech. 11 (4) (2017) 762–766.
[22] A. Seeger, Peierls barriers, kinks, and flow stress: recent progress, Z. Metalkunde 93 (2002) 760–777.
[23] S. Hara, J. Li, Adaptive strain-boost hyperdynamics simulations of stress-driven atomic processes, Phys. Rev. B 82 (2010), 184114.
[24] J.-P. Du, Y.-J. Wang, Y.-C. Lo, L. Wan, S. Ogata, Mechanism transition and strong temperature dependence of dislocation nucleation from grain boundaries: An accelerated molecular dynamics study, Phys. Rev. B 94 (2016), 104110.
[25] S. Chakraborty, J. Zhang, S. Ghosh, Accelerated molecular dynamics simulations for characterizing plastic deformation in crystalline materials with cracks, Comp. Mater. Sci. 121 (2016) 23–34.
[26] P. Hirel, ATOMSK: a tool for manipulation and converting atomic data files, Comput. Phys. Comm. 197 (2015) 212–219.

[27] M.S. Duesbery, On the non-glide stresses and their influence on the screw dislocation core in bcc cubic metals I. The Peierls stress, Proc. R. Soc. London 392 (1984) 145–173.
[28] A. Kraych, E. Clouet, L. Dezerald, L. Ventelon, F. Willaime, D. Rodney, Non-glide effects and dislocation core fields in BCC metals, npj Comp. Mater. 5 (2019) 109–116.
[29] S. Plimpton, Fast parallel algorithms for short-range molecular dynamics, J. Comp. Phys. 117 (1) (1995) 1–19.
[30] D. Farkas, C. Jones, Interatomic potentials for ternary Nb-Ti-Al alloys, Model. Simul. Mater. Sci Eng. 4 (1) (1996) 23–32.
[31] G. Henkelman, H. Jónsson, Improved tangent estimate in the nudged elastic band method for finding minimum energy paths and saddle points, J. Chem. Phys. 113 (22) (2000) 9978–9985.
[32] W.A. Spitzig, A.S. Keh, Orientation dependence of the strain-rate sensitivity and thermally-activated flow in iron single crystals, Acta Metall. 18 (9) (1970) 1021–1033.
[33] V. Celli, M. Kabler, T. Ninomiya, R. Thomson, Theory of dislocation mobility in semiconductors, Phys. Rev. 131 (1) (1963) 58–72.
[34] M. Büttiker, R. Landauer, Nucleation theory of overdamped soliton motion, Phys. Rev. Let. 43 (20) (1979) 1453–1456.
[35] J.P. Hirth, J. Lothe, Theory of Dislocations, John Wiley & Sons, New York, Chichester, 1982.
[36] F. Ackermann, H.A. Mughrabi, A. Seeger, Temperature-rate and strain-rate dependence of the flow stress of ultrapure Nb single-crystals in cyclic deformation, Acta Metall. 31 (1983) 1353–1366.
[37] D. Rodney, L. Proville, Kink-pair nucleation on dislocations under stress in the two-dimensional Frenkel-Kontorova model, Phys. Rev. B 78 (2008), 104115.
[38] M. Büttiker, E.P. Harris, R. Landauer, Thermal activation in extremely underdamped Josephson-junction circuits, Phys. Rev. B 28 (3) (1983) 1268–1275.
[39] U. Kocks, A.S. Argon, M.F. Ashby, Models for macroscopic slip, Prog. Mater. Sci. 19 (1975) 1–281.
[40] C.R. Weinberger, B.L. Boyce, C.C. Battaile, Slip planes in bcc transition metals, Int. Mater. Rev. 58 (5) (2013) 296–314.
[41] A. Stukowski, Visualization and analysis of atomistic data with OVITO-the open visualization tool, Model. Simul. Mater. Sci. Eng. 18 (2010), 015012.
[42] C. Huang, D. Perez, A.F. Voter, Hyperdynamics boost factor achievable with an ideal biased potential, J. Chem. Phys. 143 (2015), 074113.
[43] T. Zhu, J. Li, A. Samanta, A. Leach, K. Gall, Temperature and strain-rate dependence of surface dislocation nucleation, Phys. Rev. Lett. 100 (2008), 025502.
[44] L. Dezerald, D. Rodney, E. Clouet, L. Ventelon, F. Willaime, Plastic anisotropy and dislocation trajectory in BCC metals, Nat. Commun. 7 (2016) 11696.
[45] F. Maresca, D. Dragoni, G. Czanyi, N. Marzari, W.C. Curtin, Screw dislocation structure and mobility in body centred cubic Fe predicted by a Gaussian approximation potential, npj Comput. Mater. 4 (2018) 69–75.
[46] D. Rodney, L. Proville, Stress-dependent Peierls potential – influence of kink pair activation, Phys. Rev. B 79 (2009), 094108.
[47] K. Gubaev, Y. Ikeda, F. Tasnadi, J. Neugebauer, A.V. Shapeev, B. Grabowski, F. Körmann, Finite-temperature interplay of structural stability, chemical complexity, and elastic properties of bcc multicomponent alloys from *ab initio* trained machine-learning potentials, Phys. Rev. Mater. 5 (2021), 073801.
[48] B. Grabowski, Y. Ikeda, P. Srinivasan, F. Körmann, C. Freysoldt, A.I. Duff, A. Shapeev, J. Neugebauer, Ab initio vibrational free energies including anharmonicity for multicomponent alloys, npj Comput. Mater. 5 (2019) 80–86.
[49] A. Forslund, X. Zhang, B. Grabowski, A.V. Shapeev, A.V. Ruban, Ab initio simulations of the surface free energy of TiN(001), Phys. Rev. B 103 (2021), 195428.
[50] H. Conrad, Thermally activated deformation of metals, JOM 16 (7) (1964) 582–588.
[51] G. Schoeck, The activation energy of dislocation movement, Phys. Stat. Solidi 8 (2) (1965) 499–507.